PROCEEDINGS OF SCIENCE

Measurement of the transverse single spin asymmetry for forward neutron production in a wide transverse momentum range

Minho Kim[a,*] **for the RHICf collaboration**

[a] *RIKEN Nishina Center, Wako, Saitama 351-0198, Japan*

E-mail: minho.kim@riken.jp

In the high-energy polarized $p + p$ collisions, a spin-involved diffractive particle production mechanism can be understood by measuring transverse single-spin asymmetries A_{N} of forward particles that are produced at pseudorapidity larger than 6. Since A_{N} of forward neutron had only been studied in a narrow transverse momentum range of $p_{\mathrm{T}} < 0.4$ GeV/c, the RHICf Collaboration has extended the previous measurements up to 1.0 GeV/c at $\sqrt{s} = 510$ GeV to study the kinematic dependence of the neutron A_{N} in more detail. The resulting A_{N}s reach a plateau in the low longitudinal momentum fraction x_{F} range, but explicitly increase in magnitude with p_{T} in the high x_{F} range. The A_{N}s show little x_{F} dependence in the low p_{T} range. A clear x_{F} dependence is observed for higher p_{T} range in the intermediate x_{F} region. The results are consistent with the previous measurements at $\sqrt{s} = 200$ GeV, which suggests no $\sqrt{s}$ dependence of the neutron A_{N}. A theoretical model based on π and a_1 exchange between two protons could reproduce the current results only in a limited kinematic region. An additional mechanism is necessary to understand the measured neutron A_{N}s over the whole kinematic region.

25th International Symposium on Spin Physics
24-29 September 2023
Durham, NC, USA

*Speaker

PoS(SPIN2023)073

1. Introduction

In the high-energy polarized $p + p$ collisions, transverse single-spin asymmetry ($A_{\rm N}$) of the forward particle produced at pseudorapidity larger than 6 plays an important role to study the spin-dependent diffractive particle production mechanism. The $A_{\rm N}$ value is defined by a left-right cross section asymmetry as

$$A_{\rm N} = \frac{\sigma_{\rm L} - \sigma_{\rm R}}{\sigma_{\rm L} + \sigma_{\rm R}}, \tag{1}$$

where $\sigma_{\rm L\,(R)}$ is the cross section of a specific particle or event in the left (right) side of the beam polarization. The diffractive process describes the collision process in the mesonic degree of freedom.

After a large $A_{\rm N}$ for forward neutron production was discovered by a polarimeter development experiment [1] at a center-of-mass energy ($\sqrt{s}$) of 200 GeV, it had been measured by the PHENIX experiment at $\sqrt{s}$ = 62 GeV, 200 GeV, and 500 GeV [2]. The one-pion exchange model [3–5] reproduced the PHENIX results reasonably well [6] by introducing an interference between spin flip π and spin nonflip a_1 exchange. This theoretical framework predicted that the neutron $A_{\rm N}$ increased in magnitude with transverse momentum ($p_{\rm T}$) with little $\sqrt{s}$ dependence. Recently, one of the PHENIX results at $\sqrt{s}$ = 200 GeV was extracted as a function of longitudinal momentum fraction ($x_{\rm F}$) and $p_{\rm T}$ more precisely by unfolding the kinematic spectra [7] and the results were also consistent with the theoretical calculation.

Since the forward neutron $A_{\rm N}$ had only been studied in a narrow $p_{\rm T}$ range $<$ 0.4 GeV/c, the RHICf Collaboration has extended the previous measurements up to 1.0 GeV/c to study the kinematic dependence of the neutron $A_{\rm N}$ in more detail. Since $\sqrt{s}$ of the previous measurements and the RHICf experiment are different, $\sqrt{s}$ dependence of the neutron $A_{\rm N}$ could also be studied by comparing the RHICf results with those of PHENIX.

2. RHICf experiment

In June 2017, we have measured the $A_{\rm N}$ for forward neutron production in polarized $p + p$ collisions at $\sqrt{s}$ = 510 GeV by installing an electromagnetic calorimeter (RHICf detector) [8] in the zero-degree area of the STAR detector at the Relativistic Heavy Ion Collider (RHIC). A charged veto counter was also installed in front of the RHICf detector to suppress the charged hadron background. We requested large β^* value of 8 m to make the angular beam divergence small. Corresponding luminosity at $\sqrt{s}$ = 510 GeV was at a level of about 10^{31} cm^{-2}s^{-1}. We also requested 90°-rotated transversely polarized beams instead of the usual vertically polarized beams. We could measure the neutrons in a wide $p_{\rm T}$ range of $0.0 < p_{\rm T} < 1.0$ GeV/c by moving the detector vertically. See Ref. [9] for more details on the experimental conditions.

The RHICf detector consists of small and large sampling towers as shown in Fig. 1(a). A schematic drawing of the longitudinal structure of the RHICf detector is described in Fig. 1(b). Each tower is composed of 17 layers of tungsten absorbers with 1.6 interaction length in total, 16 layers of GSO scintillator plates for energy measurement, and 4 layers of 1-mm-wide GSO bar hodoscope for position measurement. The RHICf detector has 1 order of better position and $p_{\rm T}$ resolutions than the one used in the previous measurements, thereby we could measure the $A_{\rm N}$ more

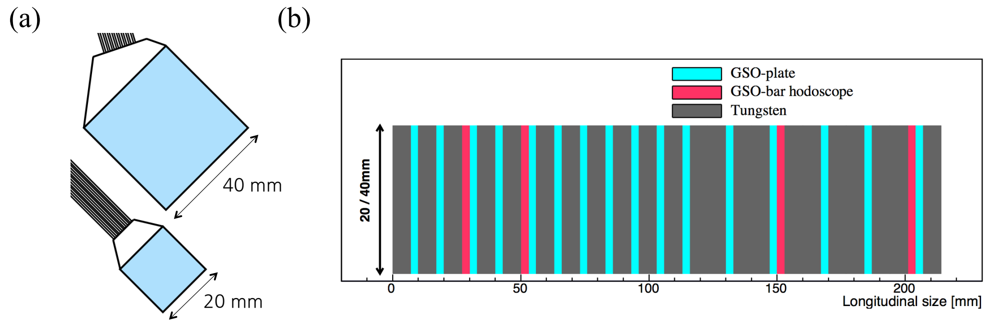

Figure 1: (a) Front view of the RHICf detector. It consists of small and large towers with 20 mm and 40 mm dimensions, respectively. (b) Longitudinal structure of the RHICf detector. Both tower have the same structure.

precisely. The neutrons were measured by a shower trigger that was operated when the energy deposits of any three consecutive GSO plates are larger than 45 MeV.

3. Data analysis

Since The shower trigger is sensitive not only to the neutron events but also to the photon events, neutron candidates were selected by using a variable called L_{2D} that described how early a particle shower was generated in the detector. Fig. 2 shows the L_{2D} distributions of neutron and photon events in the QGSJET II-04 [10] sample. Since the electromagnetic shower stops the development in the middle of the RHICf detector, the two L_{2D} distributions are clearly separated. After selecting the neutron candidates, finite photon and charged hadron backgrounds in the neutron candidates were removed. The photon contamination was estimated by fitting the L_{2D} distribution

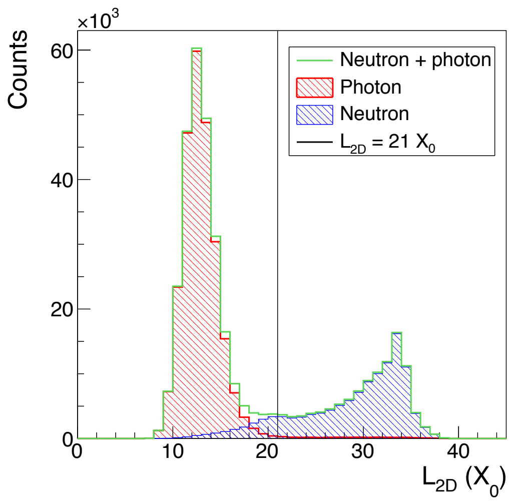

Figure 2: L_{2D} distributions of neutron and photon events in the QGSJET II-04 sample. The black line corresponds to a threshold to select the neutron candidates.

of data using those of neutron and photon events in the QGSJET II-04 sample. Each event sample was scaled so that they reproduced the data reasonably well with the minimum χ^2 value. The same method was also used to estimate and subtract the charged hadron background, but ADC distribution of the charged veto counter was fitted using neutron and charged hadron event samples. The detailed fitting results can be found in Ref. [11].

In order to precisely calculate the neutron A_N, kinematic values of neutrons, x_F, p_T, and azimuthal angle with respect to the beam axis, were unfolded using Bayesian unfolding method [12] after the background subtraction. For the prior, neutrons from 0 GeV to 255 GeV were uniformly generated on the detector. Iteration of the Bayesian unfolding was repeated until the χ^2 change between two outputs of consecutive iterations became smaller than 1. The unfolding was applied for up and down spin patterns respectively to obtain the numbers of neutrons of each spin pattern for A_N calculation.

Neutron A_Ns of a tower that did not cover the beam center were calculated by

$$A_N = \frac{1}{PD_\phi}\left(\frac{N^\uparrow - RN^\downarrow}{N^\uparrow + RN^\downarrow}\right), \tag{2}$$

where P is the beam polarization and $N^{\uparrow(\downarrow)}$ is the number of neutrons detected when the beam polarization is up (down). D_ϕ is a dilution factor estimated by

$$D_\phi = \frac{1}{N}\sum_i \sin\phi_i, \tag{3}$$

where ϕ_i is the azimuthal angle of a neutron with respect to the beam polarization in the ith event and N is the number of total detected neutrons. To calculate the neutron A_Ns of a tower that covered the beam center, azimuthal modulation of the A_N was calculated by

$$A_N = \frac{1}{P}\left(\frac{\sqrt{N^\uparrow_\phi N^\downarrow_{\phi+\pi}} - \sqrt{N^\uparrow_{\phi+\pi} N^\downarrow_\phi}}{\sqrt{N^\uparrow_\phi N^\downarrow_{\phi+\pi}} + \sqrt{N^\uparrow_{\phi+\pi} N^\downarrow_\phi}}\right), \tag{4}$$

where $N^{\uparrow(\downarrow)}_{\phi(\phi+\pi)}$ is the number of neutrons detected in azimuthal angular bin $\phi(\phi+\pi)$ when the beam polarization is up (down). The A_N was calculated by fitting the azimuthal modulation with a sine function where magnitude and phase were left as free parameters.

4. Results

Figure 3 shows the resulting A_Ns as a function of p_T and x_F. The error bars indicated by lines and boxes correspond to the statistical and systematic uncertainties, respectively. The systematic uncertainties came from the unfolding and beam center calculation processes. Figure 3(a) shows the neutron A_N as a function of p_T in three different x_F ranges. In the low-x_F range, the A_N reaches a plateau at low p_T. In the high-x_F range, the A_N does not seem to reach the plateau, but increases with increasing p_T as the π and a_1 exchange model predicted. Figure 3(b) shows the neutron A_N as a function of x_F in six different p_T ranges. The negative x_F value means that the proton beam that headed to the opposite side of the RHICf detector was polarized. In this case, the A_Ns are all consistent with zero. The positive x_F means that the proton beam that headed to the RHICf detector was polarized. In the low-p_T range < 0.2 GeV/c, the A_N reaches a plateau at low x_F, showing little x_F dependence. In the high-p_T range > 0.2 GeV/c, the A_N starts to be leveling off at higher x_F, showing a clear x_F dependence.

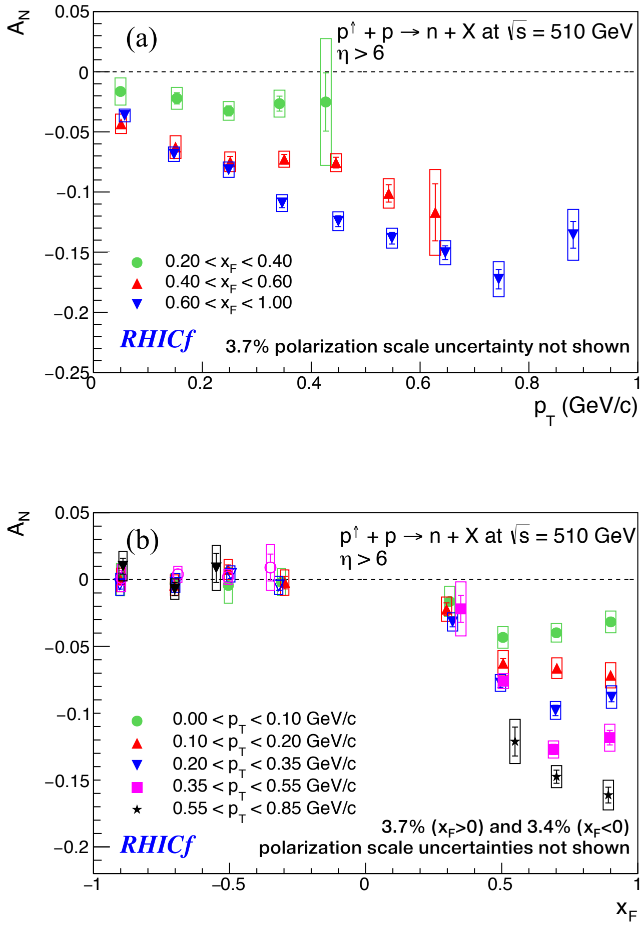

Figure 3: A_N for forward neutron production as function of (a) p_T and (b) x_F.

The RHICf results were compared with those of PHENIX in Fig. 4. Only the data points with the overlapping kinematic ranges were depicted. In the overlapping kinematic region, the two data measured by RHICf at $\sqrt{s}$ = 510 GeV and PHENIX at $\sqrt{s}$ = 200 GeV are consistent with each other. The consistency suggests no $\sqrt{s}$ dependence of the neutron A_N.

The RHICf results were also compared with the theoretical calculations based on the π and a_1 exchange between two protons in Fig. 5. In the high-x_F range, the A_Ns are mostly consistent with the model calculations. However, the model does not reproduce the other A_Ns because of the x_F dependence. The x_F dependence in the neutron A_N was observed for the first time by the RHICf experiment. In Ref. [6], spin effects by the absorptive correction can also generate finite A_N. It is also expected that other meson exchange between two protons, like ρ and a_2, could enhance the

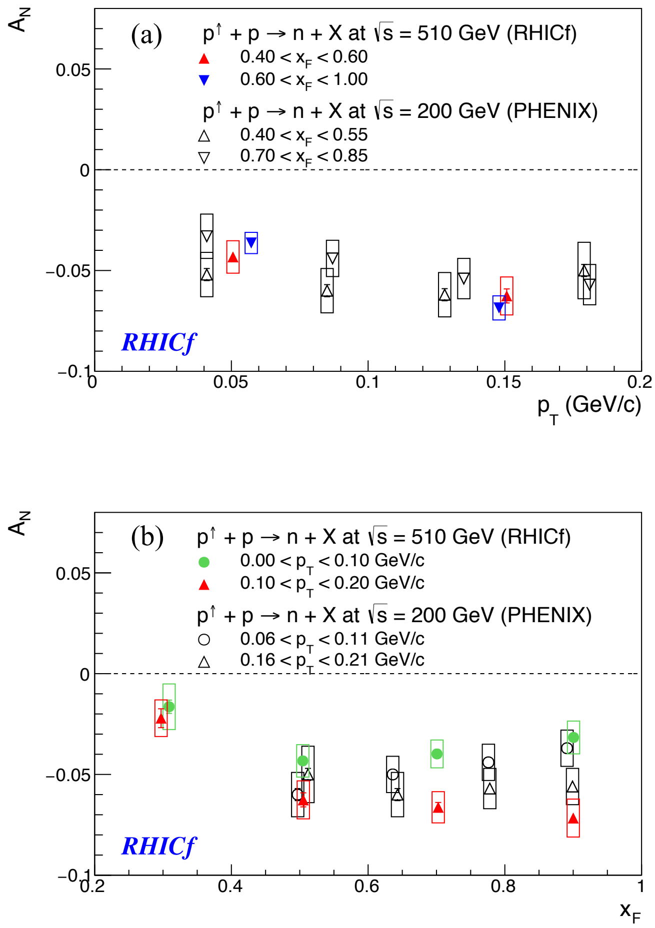

Figure 4: Comparison of the RHICf results with those of PHENIX as function of (a) p_{T} and (b) x_{F}.

A_{N} in the high-x_{F} range. Therefore, more comprehensive theoretical considerations are necessary to understand the present results.

5. Summary

In June 2017, the RHICf Collaboration has measured the neutron A_{N}s in a wide p_{T} range of $0.0 < p_{\mathrm{T}} < 1.0$ GeV/c to study the spin-dependent production mechanism of the forward neutron in detail. The resulting A_{N}s increase in magnitude with p_{T} in the high-x_{F} range. However, the A_{N}s reache a plateau in the low-x_{F} range. A clear x_{F} dependence is observed, but there are indications that the neutron A_{N}s also level off at high x_{F}. No $\sqrt{s}$ dependence was observed when the RHICf data were compared with those of PHENIX. The π and a_1 exchange model could reproduce only part of the RHICf data. Since other spin effects by the absorptive correction and ρ and a_2 exchange between two protons can also generate a finite A_{N}, additional production mechanisms need to be considered to understand the present results.

PoS(SPIN2023)073

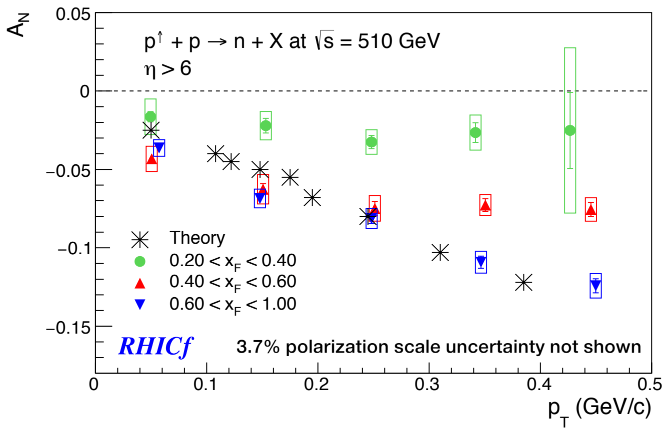

Figure 5: Comparison of the RHICf results with the theoretical calculations.

References

[1] Y. Fukao *et al.*, Phys. Lett. B **650**, 325 (2007).

[2] K. Tanida (PHENIX Collaboration), J. Phys. Conf. Ser. **295**, 012097 (2011).

[3] J. Soffer and N. A. Törnqvist, Phys. Rev. Lett. **68**, 907 (1992).

[4] U. D'Alesio and H.J. Pirner, Eur. Phys. J. A **7**, 109 (2000).

[5] B.Z. Kopeliovich, B. Povh (Heidelberg), and I.K. Potashnikova, Z. Phys. C **73**, 125 (1996).

[6] B. Z. Kopeliovich, I. K. Potashinikova, I. Schmidt, and J. Soffer, Phys. Rev. D **84**, 114012 (2011).

[7] U. A. Acharya *et al.* (PHENIX Collaboration), Phys. Rev. D **103**, 052009 (2021).

[8] RHICf Collaboration, J. Instrum. **16**, P10027 (2021).

[9] M. H. Kim *et al.* (RHICf Collaboration), Phys. Rev. Lett. **124**, 252501 (2020).

[10] S. Ostapchenko, Phys. Rev. D **83**, 014018 (2011).

[11] M. H. Kim *et al.* (RHICf Collaboration), Phys. Rev. D **109**, 012003 (2024).

[12] G. D'Agostini, Nucl. Instrum. Meth. A **362**, 487 (1995).

[13] G. Mitsuka, Private discussion based on [6] (2023).